INTERFACE

rsif.royalsocietypublishing.org

Research

Cite this article: Waldrop LD, Koehl MAR. 2016 Do terrestrial hermit crabs sniff? Air flow and odorant capture by flicking antennules. *J. R. Soc. Interface* **13**: 20150850.
http://dx.doi.org/10.1098/rsif.2015.0850

Received: 28 September 2015
Accepted: 23 December 2015

Subject Areas:
biomechanics, computational biology

Keywords:
olfaction, hermit crab, *Coenobita*, fluid dynamics, aesthetasc, flicking

Author for correspondence:
Lindsay D. Waldrop
e-mail: lwaldrop@ucmerced.edu

†Present address: School of Natural Sciences, University of California, Merced, CA, USA.

Electronic supplementary material is available at http://dx.doi.org/10.1098/rsif.2015.0850 or via http://rsif.royalsocietypublishing.org.

THE ROYAL SOCIETY PUBLISHING

Do terrestrial hermit crabs sniff? Air flow and odorant capture by flicking antennules

Lindsay D. Waldrop† and M. A. R. Koehl

Department of Integrative Biology, University of California, Berkeley, CA, USA

LDW, 0000-0001-5708-2789

Capture of odorant molecules by olfactory organs from the surrounding fluid is the first step of smelling. Sniffing intermittently moves fluid across sensory surfaces, increasing delivery rates of molecules to chemosensory receptors and providing discrete odour samples. Aquatic malacostracan crustaceans sniff by flicking olfactory antennules bearing arrays of chemosensory hairs (aesthetascs), capturing water in the arrays during downstroke and holding the sample during return stroke. Terrestrial malacostracans also flick antennules, but how their flicking affects odour capture from air is not understood. The terrestrial hermit crab, *Coenobita rugosus*, uses antennules bearing shingle-shaped aesthetascs to capture odours. We used particle image velocimetry to measure fine-scale fluid flow relative to a dynamically scaled physical model of a flicking antennule, and computational simulations to calculate diffusion to aesthetascs by odorant molecules carried in that flow. Air does not flow into the aesthetasc array during flick downstrokes or recovery strokes. Odorants are captured from air flowing around the outside of the array during flick downstrokes, when aesthetascs face upstream and molecule capture rates are 21% higher than for stationary antennules. Bursts of flicking followed by pauses deliver discrete odour samples to olfactory sensors, causing intermittency in odour capture by a different mechanism than aquatic crustaceans use.

1. Introduction

1.1. The role of sniffing in olfaction

Olfaction is the process of collecting information from chemical cues (odours) in the fluid (air or water) surrounding an organism. Many animals use this information to mediate reproduction, find food, identify competitors and avoid predation [1–4]. An important step in olfaction is odour capture, during which odorant molecules in the fluid surrounding an animal are brought into contact with a chemosensory surface. Odour capture involves moving fluid past a chemosensory surface, either by generating a fluid current across a stationary surface or by moving the surface through the fluid. This process is generally referred to as 'sniffing' and is broadly defined as any periodic movement that exposes chemosensory receptors intermittently to their fluid environment [5–8].

Sniffing enhances olfaction in a number of ways. By moving odour-bearing fluid across sensory surfaces, it increases the rate of delivery of odour molecules from the environment to the chemosensory receptors [9–11]. Sniffing delivers discrete samples of odour-bearing fluid to olfactory sensors, and thus provides distinct spatio-temporal patterns of odours to the brain [8,9,12,13] that enhance neural encoding of odour signals [7,13,14]. The periodic interruption of a continuous odour signal that sniffing provides is important for reducing habituation of chemosensory neurons [5].

Analysis of how sniffing interacts with the patchy, filamentous structure of turbulent odour plumes as animals navigate in them has shown that the

morphology and sweep of the olfactory organ affects the spatial portion of the plume sampled with each sniff, and that the temporal pattern of sniffing affects the intermittency of the odours sampled [15,16]. Therefore, before we can analyse how an animal experiences an intermittent odour plume as it navigates through it, we need to determine how it samples that plume with its olfactory organs. The first step in such an analysis is to quantify whether the sampling process itself is continuous or intermittent [17,18].

1.2. Physics of odour capture

During sniffing, two processes, convection and molecular diffusion, are responsible for bringing odour molecules in contact with the olfactory surface. Convection is the bulk movement of fluid around the sensory structure, due to both fluid currents in the environment and flow generated by the animal during odour capture [11,19]. When fluid moves relative to a solid surface (e.g. the surface of a sensory organ), the fluid in contact with the surface does not slip past the surface and a velocity gradient develops in the fluid between the surface and the free-stream flow [20,21]. The thickness of this boundary layer of sheared fluid depends on the velocity (U) of the fluid relative to the sensory surface, a characteristic length (L) of the sensory structure such as the width of a chemosensory hair, and the ratio of the viscosity to the density of the fluid (kinematic viscosity, v). Reynolds number (Re), which represents the importance of inertia to viscosity for a flow situation, relates these variables based on a non-dimensionalization of the Navier–Stokes equation:

$$Re = \frac{LU}{v}, \tag{1.1}$$

[20,21]. For $Re < 5 \times 10^5$, the thickness of the boundary layer relative to L is proportional to $Re^{-1/2}$ [21]. By increasing U, convective flow reduces the boundary layer thickness around the sensory surface.

A boundary layer interfers with the capture of odorant molecules from ambient fluid: the slowly moving layer of fluid trapped along a chemosensory surface prevents new environmental fluid containing odorant molecules from directly contacting that surface. Molecular diffusion, the second process bringing odorant molecules to sensory surfaces, is the mechanism by which odours from the environment can move across the boundary layer. An estimate of the distance that diffusion can move a molecule with a diffusion coefficient (D) during a time interval (Δt) is the RMS distance (L_{RMS}) that molecules can travel in a given direction [20]:

$$L_{RMS} = \sqrt{2D\Delta t}. \tag{1.2}$$

Therefore, the thicker the boundary layer, the longer it takes for molecules to diffuse from the fluid outside the boundary layer to a sensory surface. Since boundary layers are thinner when flow relative to a sensory surface is faster, fluid movement can reduce the distances that odorant molecules must travel to reach a sensory surface, and thus increase the rate of odorant capture.

1.3. Olfactory sampling by aquatic malacostracan crustaceans

Nasal sniffing by vertebrates moves discrete samples of air into an enclosed cavity where the chemosensory surfaces are located, whereas sniffing by aquatic malacostracan crustaceans is accomplished by flicking through the surrounding water one branch (the lateral filament) of an external antennule that bears an array of chemosensory hairs (aesthetascs) [11,17,22,23]. Flicking kinematics have been measured, and water flow around and through arrays of aesthetascs on flicking antennules has been quantified for a number of species of malacostracan crustaceans, including stomatopods [17,24], spiny lobsters [18,25–27], brachyuran crabs [23,28] and crayfish [15,29,30]. During the downstroke, the lateral filament of the antennule flicks rapidly, with $Re \approx 1$ for the aesthetascs (using hair diameter for L). At this Re, water can flow between the aesthetascs. During the slower return stroke, the aesthetascs operate at $Re \approx 0.1$ and water does not flow between these hairs, but rather a water sample is trapped within the aesthetasc array. There is enough time before the next rapid flick downstroke for odorant molecules in the trapped sample to diffuse to the surfaces of the aesthetascs [18,29–32]. During the next flick downstroke, the old sample is washed away and a new water sample flows into the aesthetasc array. Thus, antennule flicking provides a mechanism for these crustaceans to take discrete intermittent samples of odour-containing fluid without the use of an enclosed cavity [10,11].

Some malacostracan crustaceans live in intertidal or terrestrial habitats. Odour capture by antennules flicking in air can be different from in water, both because the kinematic viscosity of air is greater than water (affecting convection), and because the diffusion coefficients of molecules in air are much higher than in water (affecting rates of odorant diffusion). The consequences of these differences between air and water for odour capture by crustacean antennules have not been explored. Although moths have been shown to sniff by wing flapping that produces pulses of air flow through their feathery antennae [33], antennule flicking by crustaceans in air has not yet been shown to be sniffing.

1.4. Chemosensory antennules of terrestrial hermit crabs

We used terrestrial hermit crabs to study how malacostracan antennules sample odours in air. Terrestrial hermit crabs (family Coenobitidae, genus *Coenobita*; [34]) spend the majority of their lives on land, and only their larvae spend extended periods in water (Coenobitidae are terrestrialized to level G4, *sensu* Greenaway, 2003). Unlike most other terrestrialized malacostracans, coenobitids are adept at sensing and tracking airborne odours [35–37].

Coenobitid crabs have antennules bearing aesthetascs that differ in morphology from the hair-like aesthetascs of aquatic malacostracans [38–40]. Coenobitid crabs have leaf-like dorsoventrally flattened aesthetascs arranged like overlapping shingles on a roof (figure 1*a*,*b*), and odour molecules only have access to dendrites of chemosensory neurons through a thinned area of permeable cuticle on the outward-facing ventral surface of each aesthetasc [35,38,40]. Unlike aesthetascs on aquatic crab antennules, coenobitid aesthetascs do not bend during flicking [40].

Like marine crabs, coenobitids flick their antennules with the aesthetasc array on the upstream side of an antennule during the downstroke, and on the downstream side during the return stroke [35,36,40]. However, the flick return speed of coenobitids is twice the speed of the downstroke [40], whereas the flick return of marine crabs is

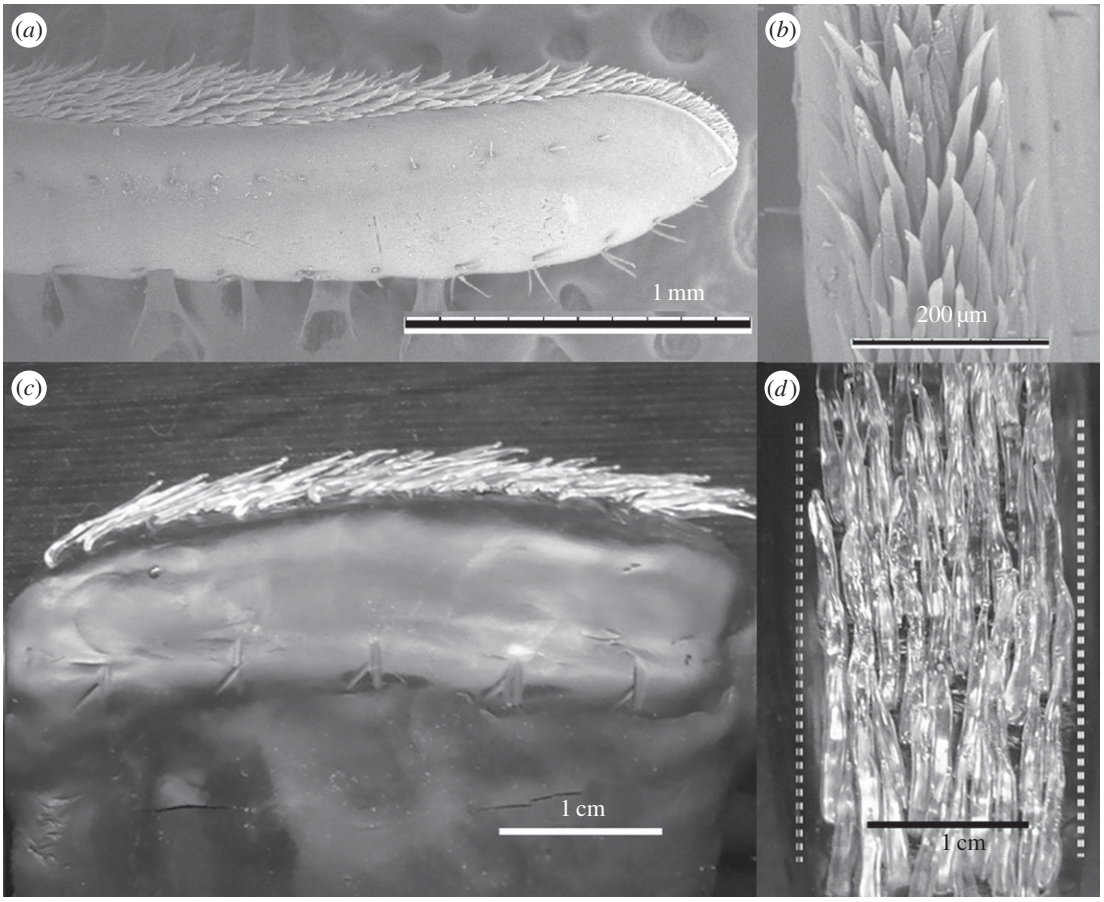

Figure 1. Scanning electron micrographs of the lateral flagellum of *C. rugosus* bearing the aesthetasc array: (*a*) lateral view and (*b*) ventral view. Dynamically scaled physical model of the lateral flagellum bearing glass aesthetascs: (*c*) side view and (*d*) ventral view. Dashed lines in (*d*) indicate the edges of the lateral filament.

much slower than the downstroke. The length of the aesthetasc-bearing region of the lateral flagellum of the antennule is greater relative to body length for coenobitid crabs than for marine crabs, and coenobitid antennules sweep greater distances through the air than antennules of similarly sized marine crabs sweep through the water [38,40].

1.5. Sniffing in air versus water

When adult *Coenobita rugosus* flick their antennules in air, they operate at $Re = 0.1$ during the downstroke and at $Re = 0.2$ during the return stroke [40]. Little fluid should move between the aesthetascs at these *Re*'s [26,41], so the antennules of these coenobitid crabs might not be able to capture discrete samples of odour-bearing air within the aesthetasc array when they flick.

Molecules diffuse much greater distances per time in air than in water. For example, the fatty acid caproic acid has a diffusion coefficient (D) approximately 7000 times higher in air ($D = 6.02 \times 10^{-6}\ \mathrm{m^2\ s^{-1}}$ [42]), than in water ($D = 7.84 \times 10^{-10}\ \mathrm{m^2\ s^{-1}}$ [43]). Higher Ds decrease the amount of time needed for molecules to traverse the boundary layer around each aesthetasc (equation (1.2)), hence the slow return strokes used by antennules of marine crustaceans that allow time for diffusion of odorants to receptors may be unnecessary for odour capture in air.

The relative importance of convection and diffusion in the transport of molecules in a fluid is given by the Péclet number,

$$Pe = \frac{UL}{D}, \tag{1.3}$$

[10,19], where L is aesthetasc diameter in the case of flicking antennules. If $Pe \gg 1$, then convective transport dominates the system, whereas if $Pe \ll 1$, diffusive transport dominates. For marine crabs flicking in water [23,28,44], $Pe \approx 1200$, indicating a reliance on convective flows to deliver odour molecules to the surfaces of aesthetascs. For terrestrial hermit crabs, $Pe \approx 0.1$ [40], suggesting that diffusion may be so rapid that air flows induced by flicking may not be necessary to deliver odour molecules to the aesthetascs of terrestrial hermit crabs.

1.6. Study objectives

The objective of this study was to determine how antennule flicking in air affects the capture of odorant molecules. We addressed this question by studying the aerodynamics of antennule flicking by the terrestrial hermit crab, *C. rugosus*. We focused on three questions:

(1) Does air flow into the aesthetasc array on the lateral filament of an antennule during the flick downstroke, and is that air sample held in the array during the return stroke?
(2) Does antennule flicking increase the rate of transport of odorant molecules to the aesthetascs by diffusion?
(3) Does the temporal pattern of flicking lead to intermittent sampling?

2. Material and methods

In this study, we use dynamically scaled physical models to investigate the fluid dynamics of antennule flicking and odour capture by a terrestrial hermit crab, *C. rugosus*. Fluid flow

around and through the aesthetasc array of the model was quantified using particle image velocimetry (PIV). The velocity vector fields of air around the aesthetascs of real antennules calculated from the PIV data were used in a computational model of convection and diffusion to estimate the capture rates of odorant molecules by the antennules flicking in air.

2.1. Dynamically scaled physical models

A physical model that was geometrically similar to the aesthetasc-bearing mid-section of the lateral flagellum of the antennules of an adult *C. rugosus* (H. Milne-Edwards 1836) was constructed based on morphometric measurements of the six largest animals described in [40] (figure 1*c*,*d*). Models of the shingle-like aesthetascs were fashioned by hand out of borosilicate glass (Kugler-Color Clear borosilicate K-100 3 mm rods) using a torch and bead-working tools. The aesthetascs were inserted into the flagellum, which was made of Scupley Premo! (Poly-form Products Co.). The model was then cured at 80°C for 45 min.

The ratios of velocities at comparable positions around a model and a real antennule are the same if they are dynamically similar, which is the case if they operate at the same Reynolds number (equation (1.1)). The aesthetascs of adult *C. rugosus* (mean width, $L = 1.5 \times 10^{-5}$ m) flicking through air (kinematic viscosity, $v = 8.55 \times 10^{-6}\,\mathrm{m^2\,s^{-1}}$ at 28°C and 100% relative humidity [45], conditions in their habitat in Moorea, French Polynesia) at a mean speed (U) of 0.061 m s^{-1} during the downstroke operate at a *Re* of 0.1, and at a mean U of 0.11 m s^{-1} during the return stroke they operate at a *Re* of 0.2 [40]. We operated our model at these aesthetasc *Re*'s by towing it through mineral oil kept at 20°C, which has a high kinematic viscosity $v = 5.8 \times 10^{-5}\,\mathrm{m^2\,s^{-1}}$. At these low *Re*'s, fluid movement due to inertia is quickly damped out by viscosity, so we assumed that the brief accelerations at the beginning and end of a flick stroke or model tow did not affect the flow during the main steady-state portion of the stroke or tow. We also calculated the Womersley number (*Wo*, the ratio of the transient inertial force of pulsatile flow to the viscous force) for antennules doing a series of flicks:

$$Wo = L\sqrt{\frac{\omega}{\nu}}, \tag{2.1}$$

where ω is the frequency of flicking (30 rad s^{-1}; see Results). The *Wo* for *C. rugosus* antennules is 0.03, which indicates that inertial effects are damped out by the fluid's viscosity and can be ignored.

The large tank and towing apparatus are described by Loudon *et al*. [46]. The model was mounted to the towing rig via an arm with its long axis oriented vertically in the tank and towed along rails above the tank and parallel to the long axis of the tank. The towing system was moved by a single-axis microstep-positioning system (MC6023, Daedal Inc., Irwin, PA, USA) and controlled by a computer running MATLAB. The model was constructed to be small enough to prevent wall effects of the tank from interfering with fluid flow around the model (for details, see [23,46]). We towed the model with the aesthetascs on the upstream side at a *Re* of 0.1 to mimic the downstroke, and with the aesthetascs on the downstream side at a *Re* of 0.2 to mimic the return stroke.

2.2. Particle image velocimetry

PIV was used to measure the fluid velocity fields around the dynamically scaled model of an antennule. The mineral oil was seeded with hollow, silver-coated glass spheres that were 11 µm in diameter (Potter Industries, Malvern, PA, USA); the spheres sank less than 2 mm during the duration of a tow and were nearly neutrally buoyant. The mineral oil was stirred prior to each experiment to ensure that the glass spheres were suspended. A horizontal sheet of light that transected the physical model at right angles to its long axis was produced by a laser (200 mW, 650 nm wavelength, Wicked Lasers) fitted with a cylindrical lens. A high-speed camera (MotionScope PCI 1000 s camera, Redlake Inc., Tucson, AZ, USA) was mounted on the towing rig directly above the model so that particle motion relative to the model was recorded. Images (480 × 420 pixels) were captured at 60 fps. Mineral oil and borosilicate glass have the same refractive index, thus the model aesthetascs were 'invisible' when immersed in the oil. Therefore, the motions of the particles carried in the oil could be video-recorded within the aesthetasc array of the physical model as well as around it. Each tow of a model was called a 'run', and three replicate runs were done per treatment.

Pairs of sequential images from the high-speed camera were then processed by PIV software (MATPIV v. 1.6.2 for MATLAB; [47]) to calculate the local fluid velocity vectors for 3009 sub-windows (8 × 8 pixels) in the fluid around the model using a method developed by Cowen & Monismith [48]. We completed PIV analysis of 60 image pairs when the model was in the middle third of the tank and the flow had reached steady-state. For each run, we calculated the mean component of oil velocity parallel to (X) and transverse to (Y) the direction of antennule motion in the plane of the laser sheet (u and v, respectively) for each sub-window ($n = 60$ image pairs). The grand mean of the u and v in each sub-window ($n = 3$ replicate runs) was calculated using the mean values from each run. The mean fluid velocity for each sub-window was the vector sum of the grand mean of u and of v for that sub-window. Mean oil velocities relative to the model were converted to air velocities relative to real antennules. All mean air velocities are reported with their standard deviations ($n = 3$ replicate runs).

2.3. Simulation of odour transport to the aesthetascs

We simulated the transport of odorant molecules to the ventral surfaces of aesthetascs on an antennule of *C. rugosus*, using a two-dimensional Markov-chain Monte Carlo simulation. To simulate convection during flicks, we used our PIV data in air with a finite-difference, forward-Euler approximation, and to simulate diffusion, we used two, one-dimensional random walks of odorant molecules. All simulations were performed in MATLAB (R2014a). The flick was divided into n time steps with duration $\Delta t = 7.82 \times 10^{-6}$ s. For each time step, the position $P(X,Y)$ of each odour molecule was advanced using a finite-difference, forward-Euler approximation based on PIV velocity vector fields:

$$X\left(t + \frac{1}{2}\Delta t\right) = X(t) + u(X(t))\Delta t \tag{2.2}$$

and

$$Y\left(t + \frac{1}{2}\Delta t\right) = Y(t) + v(Y(t))\Delta t. \tag{2.3}$$

Equation (2.2) uses u for the X component of position and equation (2.3) uses v for the Y component of position. Diffusion for each time step was advanced based on the RMS distance of diffusion (equation (1.2)) to yield the equations:

$$X(t + \Delta t) = X\left(t + \frac{1}{2}\Delta t\right) + i\sqrt{D\Delta t} \tag{2.4}$$

and

$$Y(t + \Delta t) = Y\left(t + \frac{1}{2}\Delta t\right) + i\sqrt{D\Delta t}, \tag{2.5}$$

where i was assigned the values −1, 0 or +1 based on MATLAB's pseudorandom number generator for each component of position independently. Additional details of the computational

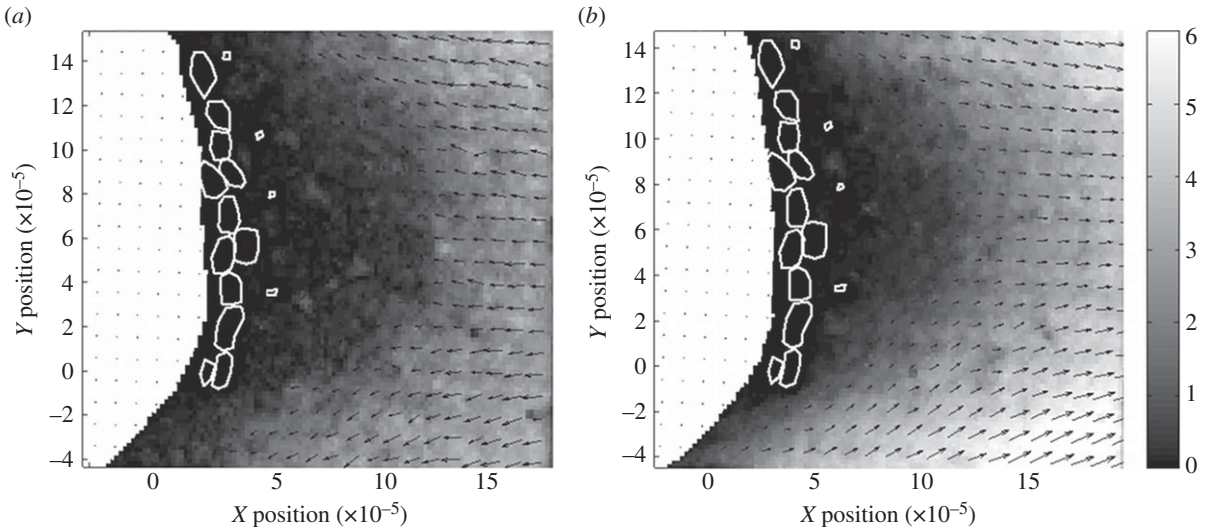

Figure 2. Maps of velocity vectors of air relative to a cross-section of the lateral filament (white region) of an antennule of *C. rugosus* calculated from PIV measurements of flow relative to a dynamically scaled model and converted to air flow around a real antennule. Positions of the aesthetascs are shown by white outlines. Black arrows indicate direction of air flow. (*a*) Downstroke of the antennule. In the diagram, the antennule moves from left to right, so air flow relative to the antennule is from right to left, which is the positive *X*-direction. (*b*) Return stroke of the antennule. In the diagram, the antennule moves from right to left, so air flow relative to the antennule is from left to right, which is the negative *X*-direction. Greyscale colours indicate mean resultant air speeds in 10^{-2} m s^{-1}. *X*- and *Y*-position scales in metres.

model, including convergence tests and a discussion of divergence, are available in the electronic supplementary material.

A patch of 100 000 simulated odorant molecules (M_{total}) was created over an area of 3.48×10^{-10} m^2 (see the electronic supplementary material for orientation); odorant molecules were evenly spaced along each axis within the area. The density of simulated odorant molecules corresponds to a concentration of 0.46 parts per billion of caproic acid in air based on mass.

We assumed that the aesthetasc array was a perfect absorber, so that any odorant molecules that crossed the boundary line of the edge of the aesthetasc were removed from the fluid and counted as captured at each time step. The total number of molecules captured was divided by the starting number of molecules to find the per cent total molecules captured, *M*. The location of the outer boundary of the physical model's aesthetasc array was chosen from raw data images (shown in the electronic supplementary material). Differences between simulations with identical parameters were so small that values of *M* were treated as deterministic and no statistical analyses were used.

We used this model to test several parameters associated with odour capture by *C. rugosus*. First, the model was used to simulate odour capture in air by a flicking antennule, in which the measured PIV velocity vector fields were used for the downstroke and return stroke, and a stationary antennule in air, in which the PIV velocity field was set to $u = 0$ (equation (2.2)) and $v = 0$ (equation (2.3)) at all points on the grid.

Second, we varied the diffusion coefficients for simulations involving both flicking and still antennules to investigate the role of diffusion in odour transport to the aesthetascs. Diffusion coefficients ranged from $D = 1 \times 10^{-10}$ to 1×10^{-5} m^2 s^{-1}, a range that includes *D*s for caproic acid in water ($D = 7.84 \times 10^{-10}$ m^2 s^{-1}) and air ($D = 6.02 \times 10^{-6}$ m^2 s^{-1}), as well as *D*s of many other common odorants.

2.4. Flicking frequencies

Videos of antennule flicking were recorded with a Phantom Miro high-speed camera at 200 fps (details in [40]). Durations of flicks and pauses between flicks were measured using frame-by-frame analysis.

3. Results

3.1. Air flow within the aesthetasc array

Velocity vectors of air moving relative to the lateral filament of an antennule of *C. rugosus* during the flick downstroke (figure 2*a*) and return stroke (figure 2*b*) were calculated from PIV measurements of flow around a physical model. During both the downstroke and return stroke, most of the fluid flowed around rather than through the aesthetasc array. The absolute values of the components of velocity parallel to the direction of antennule motion are plotted as a function of distance in the *X*-direction from the surface of the lateral filament in figure 3 for the downstroke and recovery stroke. There is almost no air motion within the aesthetasc array, while there is substantial air flow outside the array (figure 3*a*). The average speed of fluid between the aesthetascs within the array was less than 3.0×10^{-4} m s^{-1} for both the downstroke and return stroke (figure 3*b*), indicating that very little air travels through the array during flicking. The average difference between the air velocity within the aesthetascs array during the downstroke and return stroke was 3.4×10^{-5} m s^{-1}, so the net fluid displacement within the array after a flick was completed was less than the radius of an aesthetasc. Thus, a flick did not replace an old sample of air within the array with a new sample of air.

3.2. Transport of odorant molecules to the aesthetascs

To study the roles of convection and diffusion in odour capture by the aesthetascs of *C. rugosus* in air, the computational model was run for two conditions: flicking (representing capture by convection and diffusion) and still (representing capture by diffusion only for a stationary antennule in still air). The number of molecules captured per time step for the diffusivity of caproic acid in air is plotted as a function of time in figure 4*a*. At this diffusivity, the per cent of the total number of molecules in the air at the start of the

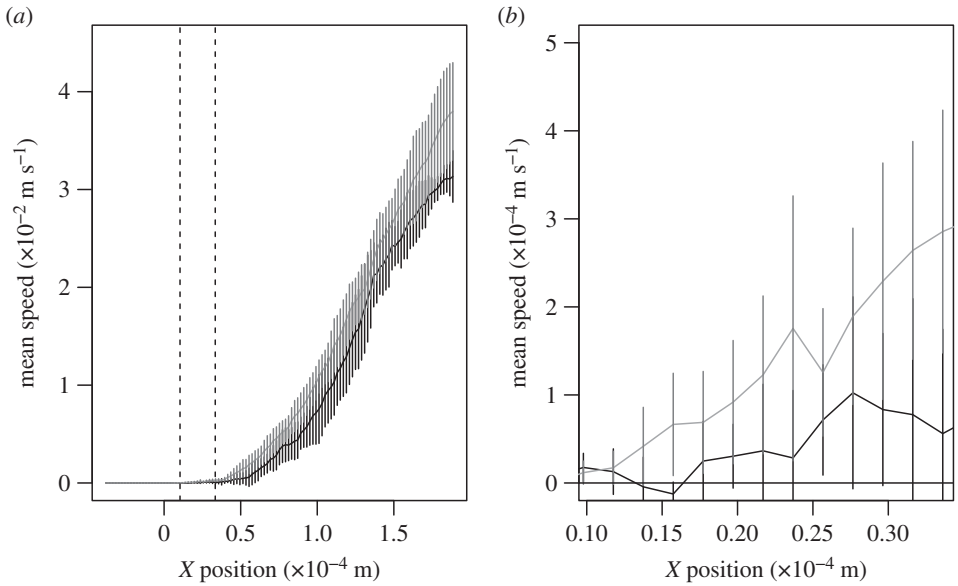

Figure 3. Mean absolute value of u (component of air velocity in the X-direction) plotted as a function of distance (X) from the surface of the lateral filament ($n = 3$ replicate runs; error bars show 1 s.d.). The bounds of the aesthetasc array are marked with dashed lines. (*a*) Mean air speeds measured for the downstroke (black) and return stroke (grey). (*b*) Mean air speeds in the spaces between the aesthetascs within the array (X positions between the dashed lines in (*a*)).

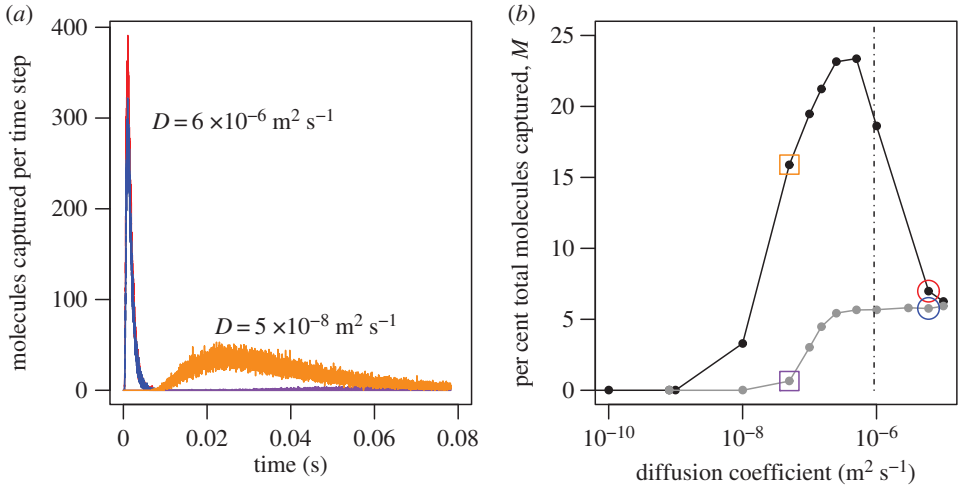

Figure 4. (*a*) Molecules captured per time step on the ventral surfaces of the aesthetascs, plotted as a function of time for flicking (red, orange) and still (blue, purple) antennules. These simulations were done for odorants with different diffusion coefficients (D): red and blue $D = 6 \times 10^{-6}$ m^2 s^{-1}, orange and purple: $D = 5 \times 10^{-8}$ m^2 s^{-1}. (*b*) Per cent total molecules captured, M, during the downstroke and return stroke versus diffusion coefficient D in m^2 s^{-1} for flicking antennules (black points and line) and still antennules (grey points and line). Two values are highlighted as they appear in (*a*): $D = 6 \times 10^{-6}$ m^2 s^{-1} marked by circles and $D = 5 \times 10^{-8}$ m^2 s^{-1} marked by squares.

simulation that were captured (M) was 6.99 for flicking, and 5.76 for still water, showing that convection increased molecule capture rates by 21%. For this case, $Pe < 1$ (equation (1.3) and diffusion is the major mechanism for moving molecules to the aesthetascs.

The diffusion coefficients (D) of large molecules are higher than for small ones, and the D for a given molecule in water is much lower than in air: Ds in air range from 10^{-7} to 10^{-5} m^2 s^{-1}, whereas Ds in water range from 10^{-11} to 10^{-9} m^2 s^{-1}. We ran additional simulations for different values of D that spanned this range (figure 4*b*). For values of D above 6.02×10^{-6} m^2 s^{-1}, diffusion was responsible for nearly all molecular capture, with convection due to flicking increasing M by a very small amount compared with the still case. In contrast, at lower diffusion coefficients in the range $2.5 \times 10^{-7} < D < 6 \times 10^{-6}$ m^2 s^{-1}, $Pe > 1$ and the M due to diffusion did not change in the still case, while M due to convection in the flicking case increased rapidly as D decreased.

Using the aesthetasc width of *C. rugosus* for L and the flicking speed for U, the D at which $Pe = 1$ is 9.2×10^{-7} m^2 s^{-1} (dotted line in figure 4*b*), which is at the low end of the range for molecules in air. Thus for most molecules in air, $Pe < 1$ and convection due to flicking only improves capture rates by a small amount. In contrast, Ds for molecules in water are several orders of magnitude lower than this, $Pe \gg 1$, and convection due to flicking can increase rates of molecule capture. For simulations with $D = 5 \times 10^{-8}$ m^2 s^{-1}, flicking (figure 4*a*, orange line and *b*, orange square) captures 24 times higher M than still simulation (figure 4*a*, purple line and *b*, purple square). However, in our simulation of a patch of odour carried past an array of aesthetascs into which no water flowed, almost no molecules were captured at very low Ds.

The diffusion coefficients at which M reached zero was an order of magnitude lower for flicking antennules ($D \approx 1 \times 10^{-9}\ m^2\ s^{-1}$) than for still antennules ($D \approx 1 \times 10^{-8}\ m^2\ s^{-1}$). No molecules were captured by an antennule with the morphology and flicking kinematics of *C. rugosus* when $D < 7.8 \times 10^{-10}\ m^2\ s^{-1}$, the diffusion coefficient of caproic acid in water.

For the majority of simulations, no molecules were captured during the return stroke because no odour-bearing water had been captured in the aesthetasc array during the downstroke, and the water velocities near the exposed ventral surfaces of the aesthetascs were very low when they were on the downstream side of the antennule during the return stroke (figure 2*b*). The only exceptions to this occurred for flicking antennules capturing large molecules in air (e.g. for $D = 1 \times 10^{-7}\ m^2\ s^{-1}$, $M \approx 1.73 \times 10^{-2}$ for the return stroke), but the number of molecules captured during the return stroke made up a tiny fraction of the total per cent captured for the entire flick. Thus, the return stroke is of little importance to odour capture by *C. rugosus* antennules.

3.3. Temporal patterns of flicking

Coenobita rugosus flicked their antennules through a volume of air of 2.2 µl per flick at a frequency of 4.8 s^{-1} (s.d. = 0.7, $n = 4$ crabs, mean of seven to 17 flicks per crab; i.e. 30 rad s^{-1}) in bursts lasting 0.77 s (s.d. = 0.22, $n = 4$ crabs), with stationary pauses between bursts of 0.84 s (s.d. = 0.21, $n = 4$ crabs).

4. Discussion

4.1. How antennule flicking in air can affect odour sampling

Antennule flicking by the terrestrial hermit crab, *C. rugosus*, should improve the chances of capturing odorant molecules in low concentrations, thereby improving the sensitivity of olfaction. Antennule flicking enables the aesthetasc array to sample a larger volume of the odour plume than would be encountered by a stationary antennule (the volume of air through which an antennule sweeps is 27 times greater than the volume of the aesthetasc array). In addition, convection due to flicking by a *C. rugosus* antennule carries odorant molecules close to the aesthetascs and increases the molecule capture rate by 21% over the capture rate due only to diffusion for a stationary antennule. Once data become available for the spatio-temporal patterns of odorant concentrations in plumes in the air flowing at the heights of *C. rugosus* antennules in their natural habitats, then we can determine the effect of this 21% increase in molecule capture rate during flicking on the temporal patterns of concentrations sampled by antennules. Using the approach of Reidenbach & Koehl [16], the temporal patterns of odorant capture at different locations in a realistic odour plume can be calculated for: (1) a stationary antennule that relies only on diffusion; (2) an antennule flicking with the timing of a *C. rugosus* and sweeping through the arc of a flick, but having no increase in molecule capture rate during the flick; and (3) an antennule flicking with the timing of a *C. rugosus* that has a 21% increase in molecule capture rate as it sweeps through its arc.

We can estimate whether flicking by antennules of *C. rugosus* results in intermittent sampling of odours by comparing the temporal patterns of flicking to the response and recovery times of olfactory neurons reported for other types of malacostracan antennules. If the time gap (t_{gap}) between successive pulses of odour is very brief (less than 0.5 s), flicker fusion is likely to occur [49,50], whereas when $t_{gap} \geq 0.5$ s, odour pulses are perceived as separate [51,52]. Therefore, within a burst of continuous flicking by *C. rugosus*, flicker fusion probably occurs and the burst can be considered as one continuous sample. However, the duration of the pauses between bursts of flicking is longer than 0.5 s, so it is likely that each burst of flicking is perceived as a separate pulse. The responses of olfactory receptor cells of *C. rugosus* antennules should be measured, but based on what is known about similar neurons in other malacostracans, it is likely that each burst of flicking by *C. rugosus* should be considered as a single sniff that lasts about 0.8 s, with a t_{gap} until the next sniff of about 0.8 s.

Our results indicate that flicking by the antennules of hermit crabs accomplishes the two functions of sniffing [9]: (1) during each rapid flick downstroke, the rate of delivery of odour molecules to the aesthetascs is increased; and (2) each burst of flicks followed by a pause delivers a discrete sample of odour to olfactory sensors. The next stage of research will be to explore how taking 0.8 s samples of air in the small region swept by an antennule every 1.6 s affects the temporal patterns of odour concentrations intercepted. Turbulent odour plumes in natural environments are made up of filaments of odour swirling in odour-free fluid, so concentrations sampled at a point are intermittent. Comparison of aquatic crabs and lobsters, which flick their antennules at different frequencies, showed that the temporal patterns of odorant concentrations they intercept at the same positions in the same odour plume are different [16], thus flicking filters the temporal patterns of odour concentrations sampled by an animal. Turbulent plumes in air tend to have wider, lower concentration odour filaments than do plumes in water [53,54], and antennule flicks of terrestrial coenobitid crabs last longer and sweep through much larger volumes of fluid than do flicks by marine crabs [40]. It will be interesting to compare the temporal filtering of odour concentrations by antennules flicking in different ways in turbulent plumes in wind versus in water currents.

4.2. Odour sampling by flicking antennules of terrestrial hermit crabs versus aquatic malacostracans

Both aquatic malacostracans and terrestrial hermit crabs sniff by flicking their antennules, but the mechanisms that lead to intermittent sampling are different. The process of flicking by aquatic malacostracans is divided into two parts, each with its own function: (1) the rapid downstroke, during which water flows between the aesthetascs, captures a water sample containing odour molecules, and (2) the slower return stroke holds the water sample within the aesthetasc array and allows time for odour molecules to diffuse to the surfaces of the permeable hair-like aesthetascs (reviewed by Koehl [10,11]).

The sniffing mechanism used by the antennules of aquatic malacostracans, which depends on changes in the leakiness of the aesthetasc array between the downstroke and return stroke, does not operate for terrestrial hermit crabs. Odorant molecules diffuse through air much more rapidly than they do through water, so retention of an air sample around the aesthetascs to permit time for odorant diffusion to aesthetasc

surfaces is not necessary and does not occur for antennules of *C. rugosus*. During flicking in air by *C. rugosus*, there is very little air flow within the aesthetasc array, both during the downstroke and during the return stroke (figure 3*b*). Furthermore, odorants are only taken up at the exposed ventral surfaces of the leaf-like aesthetascs of *C. rugosus* where the cuticle is permeable to the molecules, thus odorants are captured from the air flowing around the outside of the aesthetasc array, not from the air between aesthetascs. Convection due to flicking by a *C. rugosus* antennule carries odorant molecules close to the aesthetascs and increases the molecule capture rate by 21% over the capture rate due only to diffusion for a stationary antennule. Bursts of flicking with this increased molecule capture rate are separated by pauses with lower capture rates, thus leading to intermittent sampling of ambient odour concentrations.

Our simulations of odour capture by *C. rugosus* antennules flicking in water (i.e. odorants with *D*s of 10^{-11} to $10^{-9}\,m^2\,s^{-1}$) showed that the aesthetascs capture very few or no molecules (figure 4*b*). Thus, selective pressure to maintain an aquatic antennule morphology and sniffing mechanism was most likely removed when terrestrialization occurred (see [35,38,55]).

4.3. Comparison to other terrestrialized members of Tetraconata (crustaceans and insects)

Coenobitid crabs likely represent one of the few terrestrialized groups of malacostracan crustaceans that retain the olfactory function of their antennules on land. Studies of members of other lineages of terrestrial crustaceans within the Tetraconata have not revealed olfactory-guided behaviour in air [35,56]. One exception to this is terrestrial isopods, which exhibit weak olfactory-guided behaviour in air; their antennules are reduced in size and number of aesthetascs compared with those of aquatic isopods [56]. Desert isopods lack aesthetascs, do not flick their antennules and the areas of the brain responsible for processing olfactory information have been functionally lost [36].

Like coenobitid crabs, insects are adept at tracking odour plumes in air [57]. Insects have lost their first antennae and secondarily developed chemosensory sensilla on their second antennae, thus the olfactory capture structures of coenobitid crabs and insects are not homologous [35,36]. Studies of sniffing by insects in air are few. Pulses of air flow created by wing flapping of moths increased the leakiness of their plumose antennae intermittently, thereby enabling them to sniff [33]. The flow intermittency induced by beating wings plays an important role for conditioned behavioural responses to odorants by hawk moths [13]. However, for insect antennae that are not feathery, the air movement produced by beating wings and the slipstreams of flight can also provide a way to increase convective transport of molecules to chemosensory sensilla [13,33,58], just as the air convection during *C. rugosus* flicking enhances molecule capture rates.

Data accessibility. All data are available at FigShare: http://dx.doi.org/10.6084/m9.figshare.1558300.

Competing interests. We declare we have no competing interests.

Acknowledgements. Special thanks to Laura Miller, Shilpa Khatri and Dennis Evangelista for assistance with the computational model and manuscript editing; Jonaya Leek and The Crucible Art Collective for assistance in constructing the physical model; U.C. Berkeley's CiBER for equipment; the Biomechanics Group in the Department of Integrative Biology at U.C. Berkeley; and the U.N.C. Research Computing Center for computational time.

Funding. This work was supported by a James S. McDonnell Foundation grant, and the Virginia and Robert Gill Chair (to M.A.R.K.); by a National Science Foundation Integrative Graduate Education and Research Training grant DGE-0903711 (to R. Full, M.A.R.K., R. Dudley and R. Fearing); by a Reskteco and Gray Fellowship from the University of California, Berkeley, a Sigma-Xi Grant-in-Aid of Research, and a Crucible Art Collective Scholarship (to L.D.W.); and by a National Science Foundation Research and Training in Mathematics grant no. 5-54990-2311 (to R. McLaughlin, R. Camassa, L. Miller, G. Forest and P. Mucha).

References

1. Hazlett B. 1969 Individual recognition and agonistic behaviour in *Pagurus bernhardus*. *Nature* **222**, 268–269. (doi:10.1038/222268a0)
2. Gleeson R. 1980 Pheromone communication in the reproductive behavior of the blue crab, *Callinectes sapidus*. *Mar. Behav. Physiol.* **7**, 119–134. (doi:10.1080/10236248009386976)
3. Gherardi F, Tricarico E, Atema J. 2005 Unraveling the nature of individual recognition by odor in hermit crabs. *J. Chem. Ecol.* **31**, 2877–2896. (doi:10.1007/s10886-005-8400-5)
4. Gherardi F, Tricarico E. 2007 Can hermit crabs recognize social partners by odors? And why? *Mar. Freshwater Behav. Physiol.* **40**, 201–212. (doi:10.1080/10236240701562297)
5. Dethier V. 1987 Sniff, flick, and pulse, an appreciation of interruption. *Proc. Am. Phil. Soc.* **131**, 159–174.
6. Ache B. 1991 Phylogeny of smell and taste. In *Smell and taste in health and disease* (ed. T Getchell), pp. 3–18. New York, NY: Raven Press.
7. Mainland J, Sobel N. 2006 The sniff is part of the olfactory percept. *Chem. Senses* **31**, 181–196. (doi:10.1093/chemse/bjj012)
8. Schoenfeld T. 2006 Special issue: what's in a sniff? The contributions of odorant sampling to olfaction. *Chem. Senses* **31**, 91–92. (doi:10.1093/chemse/bjj014)
9. Kepecs A, Powell I, Weissburg M. 2006 The sniff as a unit of olfactory processing. *Chem. Senses* **31**, 167–179. (doi:10.1093/chemse/bjj016)
10. Koehl M. 2006 The fluid mechanics of arthropod sniffing in turbulent odor plumes. *Chem. Senses* **31**, 93–105. (doi:10.1093/chemse/bjj009)
11. Koehl M. 2011 Hydrodynamics of sniffing by crustaceans. In *Chemical communication in crustaceans* (eds T Breithaupt, M Theil), pp. 85–102. New York, NY: Springer.
12. Vickers N. 2006 Winging it: moth flight behavior and responses to olfactory neurons are shaped by pheromone plume dynamics. *Chem. Senses* **31**, 155–166. (doi:10.1093/chemse/bjj011)
13. Daly K, Kalwar F, Hatfield M, Staudacher E, Bradley S. 2013 Odor detection in *Manduca sexta* is optimized when odor stimuli are pulsed at a frequency matching the wing beat during flight. *PLoS ONE* **8**, e81863. (doi:10.1371/journal.pone.0081863)
14. Brennan P. 2008 Why sniff? *Chem. Senses* **33**, 597–598. (doi:10.1093/chemse/bjn036)
15. Mead K, Wiley M, Koehl M, Koseff J. 2003 Fine-scale patterns of odour encounter by the antennules of mantis shrimp tracking turbulent plumes in wave-affected and unidirectional flow. *J. Exp. Biol.* **206**, 181–193. (doi:10.1242/jeb.00063)
16. Reidenbach M, Koehl M. 2011 The spatial and temporal patterns of odors sampled by lobsters and crabs in a turbulent plume. *J. Exp. Biol.* **214**, 3138–3153. (doi:10.1242/jeb.057547)
17. Mead K, Koehl M. 2000 Stomatopod antennule design: the asymmetry, sampling efficiency and ontogeny of olfactory flicking. *J. Exp. Biol.* **203**, 3795–3808.

18. Reidenbach M, George N, Koehl M. 2008 Antennule morphology and flicking kinematics facilitate odour sampling by the spiny lobster, *Panulirus argus*. *J. Exp. Biol*. **211**, 2849–2858. (doi:10.1242/jeb.016394)
19. Moore P, Crimaldi J. 2004 Odor landscapes and animal behavior: tracking odor plumes in different physical worlds. *J. Mar. Systems* **49**, 55–64. (doi:10.1016/j.jmarsys.2003.05.005)
20. Denny M. 1993 *Air and water: the biology of life's media*. Princeton, NJ: Princeton University Press.
21. Vogel S. 1994 *Life in moving fluids: the physical biology of flow*. Princeton, NJ: Princeton University Press.
22. Schmidt B, Ache B. 1979 Olfaction: responses of a decapod crustacean are enhanced by flicking. *Science* **205**, 204–206. (doi:10.1126/science.205.4402.204)
23. Waldrop L, Hann M, Henry A, Kim A, Punjabi A, Koehl M. 2015 Ontogenetic changes in the olfactory antennules of the shore crab, *Hemigrapsus oregonensis*, maintain sniffing function during growth. *J. R. Soc. Interface* **12**, 20141077. (doi:10.1098/rsif.2014.1077)
24. Mead K, Koehl M, O'Donnell M. 1999 Stomatopod sniffing: the scaling of chemosensory sensillae and flicking behavior with body size. *J. Exp. Mar. Biol. Ecol*. **241**, 235–261. (doi:10.1016/S0022-0981(99)00087-8)
25. Goldman J, Koehl M. 2001 Fluid dynamic design of lobster olfactory organs: high speed kinematic analysis of antennule flicking by *Panulirus argus*. *Chem. Senses* **26**, 385–398. (doi:10.1093/chemse/26.4.385)
26. Koehl M. 2001 Transitions in function at low Reynolds number: hair-bearing animal appendages. *Math. Methods Appl. Sci*. **24**, 1523–1532. (doi:10.1002/mma.213)
27. Goldman J, Patek S. 2002 Two sniffing strategies in palinurid lobsters. *J. Exp. Biol*. **205**, 3891–3902.
28. Waldrop L, Reidenbach M, Koehl M. 2015 Flexibility of crab chemosensory sensilla enables flicking antennules to sniff. *Biol. Bull*. **229**, 185–198.
29. Pravin S, Mellon D, Reidenbach M. 2012 Micro-scale fluid and odorant transport to antennules of the crayfish, *Procambarus clarkii*. *J. Comp. Physiol. A* **198**, 669–681. (doi:10.1007/s00359-012-0738-x)
30. Nelson J, Mellon D, Reidenbach M. 2013 Effects of antennule morphology and flicking kinematics on flow and odor sampling by the freshwater crayfish, *Procambarus clarkii*. *Chem. Senses* **38**, 729–741. (doi:10.1093/chemse/bjt041)
31. Stacey M, Mead K, Koehl M. 2002 Molecule capture by olfactory antennules: mantis shrimp. *J. Math. Biol*. **44**, 1–30. (doi:10.1007/s002850100111)
32. Schuech R, Stacey M, Barad M, Koehl M. 2012 Numerical simulations of odorant detection by biologically inspired sensor arrays. *Bioinspiration Biomimetics* **7**, 016001. (doi:10.1088/1748-3182/7/1/016001)
33. Loudon C, Best B, Koehl M. 2000 Sniffing by a silkworm moth: wing fanning enhances air penetration through and pheromone interception by antennae. *J. Exp. Biol*. **203**, 2977–2990.
34. Ahyong S, Schnabel K, Mass E. 2009 Anomuran phylogeny: new insights from molecular data. In *Decapod crustacean phylogenetics* (eds J Martin, K Randall, D Felder), pp. 399–414. Boca Raton, FL: CRC Press.
35. Stensmyr M, Erland S, Hallberg E, Wallen R, Greenaway P, Hansson B. 2005 Insect-like olfactory adaptations in the terrestrial giant robber crab. *Curr. Biol.* **15**, 116–121. (doi:10.1016/j.cub.2004.12.069)
36. Harzsch S, Rieger V, Krieger J, Seeuth F, Strausfeld N, Hansson B. 2011 Transition from marine to terrestrial ecologies: changes in olfactory and tritocerebral neuropils in land-living isopods. *Arthropod. Struct. Dev*. **40**, 244–257. (doi:10.1016/j.asd.2011.03.002)
37. Krång A, Knaden M, Steck K, Hansson B. 2012 Transition from sea to land: olfactory function and constraints in the terrestrial hermit crab *Coenobita clypeatus*. *Proc. R. Soc. B* **279**, 3510–3519. (doi:10.1098/rspb.2012.0596)
38. Ghiradella F, Case J, Cronshaw J. 1968 Structure of aesthetascs in selected marine and terrestrial decapods—chemoreceptor morphology and environment. *Am. Zool*. **8**, 603–621. (doi:10.1093/icb/8.3.603)
39. Mellon D, Reidenbach M. 2012 Fluid mechanical problems in crustacean active chemoreception. In *Frontiers in sensing: from biology to engineering* (eds F Barth, J Humphrey, M Srinivasan). Vienna, Austria: Springer.
40. Waldrop L, Bantay R, Nguyen Q. 2014 Scaling of olfactory antennae of the terrestrial hermit crabs *Coenobita rugosus* and *Coenobita perlatus* during ontogeny. *PeerJ* **2**, e535. (doi:10.7717/peerj.535)
41. Cheer A, Koehl M. 1987 Paddles and rakes—fluid flow through bristled appendages of small organisms. *J. Theor. Biol*. **129**, 17–39. (doi:10.1016/S0022-5193(87)80201-1)
42. Lugg G. 1968 Diffusion coefficients of some organic and other vapors in air. *Anal. Chem*. **40**, 1072–1077. (doi:10.1021/ac60263a006)
43. Hayduk W, Laudie H. 1974 Prediction of diffusion coefficients for nonelectrolytes in dilute aqueous solutions. *AIChE J*. **20**, 611–615. (doi:10.1002/aic.690200329)
44. Waldrop L. 2013 Ontogenetic scaling of the olfactory antennae and flicking behavior of the shore crab, *Hemigrapsus oregonensis*. *Chem. Senses* **38**, 541–550. (doi:10.1093/chemse/bjt024)
45. Tracy C, Welch W, Porter W. 1980 *Properties of air: a manual for use in biophysical ecology*. Technical report no. 3, Laboratory for Biophysical Ecology, University of Wisconsin, Madison, WI, USA.
46. Loudon C, Best B, Koehl M. 1994 When does motion relative to neighboring surfaces alter the flow-through arrays of hairs. *J. Exp. Biol*. **193**, 233–254.
47. Sveen J. 2004 *An introduction to MatPIV v. 1.6.1: mechanics and applied mathematics*, 2nd edn. Oslo, Norway: Department of Mathematics, University of Oslo.
48. Cowen E, Monismith S. 1997 A hybrid digital particle tracking velocimetry technique. *Exp. Fluids* **22**, 199–211. (doi:10.1007/s003480050038)
49. Gomez G, Voigt R, Atema J. 1994 Frequency filter properties of lobster chemoreceptor cells determined with high-resolution stimulus measurement. *J. Comp. Physiol. A* **174**, 803–811. (doi:10.1007/BF00192730)
50. Gomez G, Voigt R, Atema J. 1999 Temporal resolution in olfaction III: flicker fusion and concentration-dependent synchronization with stimulus pulse trains of antennular chemoreceptor cells in the American lobster. *J. Comp. Physiol. A* **185**, 427–436. (doi:10.1007/s003590050403)
51. Gomez G, Atema J. 1996 Temporal resolution in olfaction: stimulus integration time of lobster chemoreceptor cells. *J. Exp. Biol*. **199**, 1771–1779.
52. Page J, Dickman B, Webster D, Weissburg M. 2011 Getting ahead: context-dependent responses to odorant filaments drive along-stream progress during odor tracking in blue crabs. *J. Exp. Biol*. **214**, 1498–1512. (doi:10.1242/jeb.049312)
53. Murlis J, Elkinton J, Carde R. 1992 Odor plumes and how insects use them. *Annu. Rev. Entomol*. **37**, 505–532. (doi:10.1146/annurev.en.37.010192.002445)
54. Weissburg M. 2000 The fluid dynamical context of chemosensory behavior. *Biol. Bull*. **198**, 188–202. (doi:10.2307/1542523)
55. Harzsch S, Hansson B. 2008 Architecture of the central olfactory pathway in a terrestrial hermit crab with a superb aerial sense of smell, *Coenobita clypeatus* (Crustacea, Anomura, Coenobitidae). *J. Morphol*. **269**, 1463.
56. Hansson B, Stensmyr M. 2011 Evolution of insect olfaction. *Neuron* **72**, 698–711. (doi:10.1016/j.neuron.2011.11.003)
57. Settles G. 2005 Sniffers: Fluid-dynamic sampling for olfactory trace detection in nature and homeland security—the 2004 Freeman Scholar Lecture. *J. Fluids Eng*. **127**, 189–218. (doi:10.1115/1.1891146)
58. Schneider R, Price B, Moore P. 1998 Antennal morphology as a physical filter of olfaction: temporal tuning of the antennae of the honeybee, *Apis mellifera*. *J. Insect Physiol*. **44**, 677–684. (doi:10.1016/S0022-1910(98)00025-0)